DYNAMIC RESPONSE ANALYSIS OF h-FGS PLATES SUBJECTED TO CONSECUTIVE BLAST LOADING

Manh Tuan Duong[1,*]

[1]*Institute of Technical Engineering, Sa Doi Street, Hanoi, Vietnam*

Abstract

The main aim of this work is to use a finite element method (FEM) based on Shi's third-order shear deformation plate theory (TSDT) to study the dynamic response of sandwich plates subjected to consecutive blast loading. The sandwich plate has an auxetic honeycomb core and two different functionally graded materials (FGMs) skin layers (so-called h-FGS plates). The honeycomb core helps significantly reduce the weight of the sandwich structures as well as enhance vibration absorption. The governing equation is derived from Hamilton's principle. After verifying the present approach, the effect of input parameters on the dynamic response of h-FGS plates is carried out in detail. The obtained results are expected to be useful for calculating and designing h-FGS plates in practical engineering.

Keywords: *Dynamic response; FGM; auxetic honeycomb; FEM.*

1. Introduction

A sandwich structure typically consists of a low-density core layer embedded between two relatively thin but stiff coating layers [1]. The outstanding properties of this structure are high specific strength, light weight and excellent absorption capacity, etc. Therefore, it is increasingly widely applied in various fields such as civil, aerospace, defence and maritime.

The core of sandwich structures is normally thick and made of low-density materials to provide high flexural stiffness and overall light weight. Thus, foams, honeycombs, or honeycomb structures filled with foam are usually used to fabricate the core. The behaviour of sandwich plates/shells with foam/honeycomb has been reported in the works of Wan et al. [2], Zhang et al. [3], Zhu et al. [4], Duc et al. [5, 6], Cong et al. [7], Tran et al. [8, 9], Nguyen et al. [10]. On the other hand, the FGM with high strength and high-temperature resistance is an ideal candidate for skin layers of sandwich structures [11-14].

Blast loading is a high-intensity, short-term load that poses a significant risk to weapons, equipment, and individuals [15]. The effect of explosive loads on the mechanical behaviour of the structure can be found in the literature [16-18]. In more recent research, Duc et al. [19, 20] investigated the vibration of FGM plates under explosive loading using an analytical method. Besides, Qi et al. [21] also employed an

* Email: tuanmanhvkt123@gmail.com
DOI: 10.56651/lqdtu.jst.v7.n01.826.sce

exact solution to examine the vibration characteristics of curved sandwich plates under blast loading.

Nowadays, the application of FEM in mechanical analysis has become popular, using the Q4 element is easy to conduct on computers and achieve initial results in analyzing structures. This article uses the Q4 element with seven degrees of freedom (DOFs) per node to establish the governing equation of h-FGS plates. It avoids "the shear-locking" phenomenon in the classical Q4 element. Then, a few examples are conducted to demonstrate the effectiveness of the proposed method. Moreover, the numerical and graphical results also help present the effect of geometrical parameters and material properties on the dynamic response of h-FGS plates.

2. Computational model

2.1. The h-FGS plate model

Considering the h-FGS plate with the dimension of $a \times b \times h$ as displayed in Fig. 1. The sandwich plate includes three layers: an auxetic honeycomb core and two face-sheet layers made of two different FGMs, which are FGM-1 at the bottom layer and FGM-2 at the top layer. The thickness of the bottom layer, the core layer and the top layer are h_1, h_2, h_3, respectively. A group of $h_1 - h_2 - h_3$ is used to denote the skin-core-skin thickness ratio.

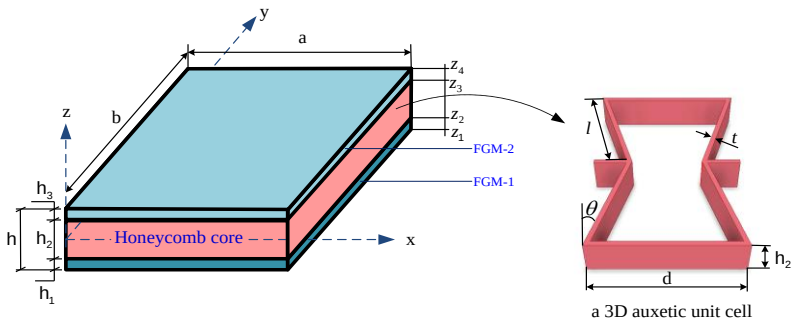

Fig. 1. The h-FGS plate model.

The effective properties of the material through thickness are defined by [22]:

$$\begin{cases} P(z) = P_b + (P_c - P_b)\left(\dfrac{z - z_1}{z_2 - z_1}\right)^n & z \in [z_1; z_2] \\ P(z) = P_{hc} & z \in [z_2; z_3] \\ P(z) = P_b + (P_c - P_b)\left(\dfrac{z - z_4}{z_3 - z_4}\right)^n & z \in [z_3; z_4] \end{cases} \quad (1)$$

where P_b, P_t are respectively the material properties, i.e., elastic moduli, mass density and Poisson's ratio of the bottom and top surfaces of each layer; *n* is the power-law indexes of FGM-1 and FGM-2, respectively; P_{hc} denotes elastic modulus, mass density and Poisson's ratio of an auxetic honeycomb core. The constituent of three layers of the h-FGS plate is described in Table 1 and mechanical properties as provided in Table 2.

Table 1. The construction and constituent of h-FGS plates [23]

The bottom layer (FGM-1)	Honeycomb core	The top layer (FGM-2)
SUS304/Al	Al	Al/Al_2O_3

Table 2. The mechanical properties of component materials [23]

Component materials	Elastic modulus (GPa)	Mass densities (kg/m^3)	Poisson's ratio
Al_2O_3	380	3800	0.3
Al	70	2707	0.3
SUS304	207	8166	0.3
ZrO_2	151	3000	0.3

The effective elastic properties (P_{hc}) of an auxetic honeycomb core are defined by [23]:

$$
\begin{aligned}
&E_1^c = E_0 \frac{\lambda_3^2(\lambda_1 - \sin\theta)}{\cos\theta\left[\cos^2\theta + \lambda_3^2(\lambda_1 + \sin^2\theta)\right]}; E_1^c = E_0 \frac{\lambda_3^2}{\cos\theta(\lambda_1\text{-}\sin\theta)(\lambda_3^2 + \tan^2\theta)};\\
&G_{12}^c = E_0 \frac{\lambda_3^2}{\lambda_1(1+2\lambda_1)\cos\theta}; G_{13}^c = G_0 \frac{\lambda_3}{2\cos\theta}\left[\frac{\lambda_1 - \sin\theta}{1+2\lambda_1} + \frac{\lambda_1 + 2\sin^2\theta}{2(\lambda_1 - \sin\theta)}\right];\\
&G_{23}^c = G_0 \frac{\lambda_3\cos\theta}{\lambda_1 - \sin\theta}; \rho^c = \rho_0 \frac{\lambda_3(\lambda_1 + 2)}{2\cos\theta(\lambda_1 - \sin\theta)};\\
&\nu_{12}^c = \frac{-\sin\theta(1-\lambda_3^2)(\lambda_1 - \sin\theta)}{\left[\cos^2\theta + \lambda_3^2(\lambda_1 + \sin^2\theta)\right]}; \nu_{21}^c = \frac{-\sin\theta(1-\lambda_3^2)}{(\lambda_1\text{-}\sin\theta)(\lambda_3^2 + \tan^2\theta)}.
\end{aligned}
\tag{2}
$$

where $\lambda_1 = d/l$ and $\lambda_3 = t/l$ with the remaining dimensions of an auxetic unit cell as shown in Fig. 1.

The consecutive blast loading can be modelled as two shock wave layers acting independently and uniformly distributed across the entire surface of the plate. The time difference between these two wave layers is denoted as $\Delta t = 0.005\text{s}$, each wave layer having the pressure function $p_i(t)$, $i = 1, 2$. The mathematical expression for this model is shown in Fig. 2 and can be defined by the following formula [23] (3):

$$p(t)=\begin{cases} p_1(t)=p_2(t)=1.8P_m e^{-\mu t/\tau}F(t) \\ F(t)=\begin{cases}(1-t/\tau) \text{ with } 0\le t\le\tau \\ 0 \quad\quad \text{with } t\ge\tau\end{cases}\end{cases} \tag{3}$$

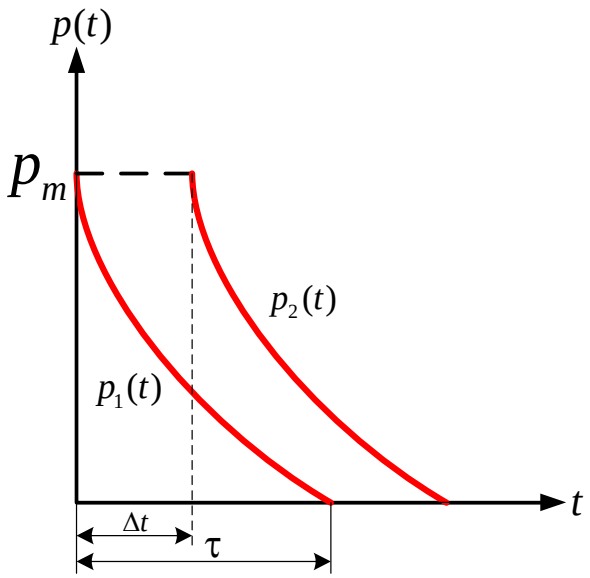

Fig. 2. The consecutive blast loading function.

in which $P_m=280\,\text{KPa}$ is the maximum blast load; $\mu=1.7$ is the decay parameter; $\tau=0.01\text{s}$ is positive phase duration.

2.2. Shi's TSDT

Applying Shi's TSDT, the displacement field of sandwich plates is [24]:

$$\begin{cases} u(x,y,z)=u_0(x,y)+\frac{5}{4}(z-\frac{4}{3h^2}z^3)\varphi_x(x,y)+(\frac{1}{4}z-\frac{5}{3h^2}z^3)w_{0,x} \\ v(x,y,z)=v_0(x,y)+\frac{5}{4}(z-\frac{4}{3h^2}z^3)\varphi_y(x,y)+(\frac{1}{4}z-\frac{5}{3h^2}z^3)w_{0,y} \\ w(x,y,z)=w_0(x,y) \end{cases} \tag{4}$$

where u_0, v_0, w_0 φ_x and φ_y are displacement variables.

Now, the strain field can be inferred by [24]:

$$\boldsymbol{\varepsilon}=\boldsymbol{\varepsilon}_m+z\boldsymbol{\kappa}_1+z^3\boldsymbol{\kappa}_2;\ \boldsymbol{\gamma}=\boldsymbol{\gamma}_0+z^2\boldsymbol{\gamma}_1 \tag{5}$$

in which

$$\boldsymbol{\varepsilon}_m = \begin{Bmatrix} u_{0,x} \\ v_{0,y} \\ u_{0,y} + v_{0,x} \end{Bmatrix}; \boldsymbol{\kappa}_1 = \frac{1}{4}\begin{Bmatrix} 5\varphi_{x,x} + w_{0,xx} \\ 5\varphi_{y,y} + w_{0,yy} \\ 5\varphi_{x,y} + 5\varphi_{y,x} + 2w_{0,xy} \end{Bmatrix};$$
$$\boldsymbol{\kappa}_2 = -\frac{5}{3h^2}\begin{Bmatrix} \varphi_{x,x} + w_{0,xx} \\ \varphi_{y,y} + w_{0,yy} \\ \varphi_{x,y} + \varphi_{y,x} + 2w_{0,xy} \end{Bmatrix}; \boldsymbol{\gamma}_0 = \frac{1}{4}\begin{Bmatrix} w_{0,y} + \varphi_y \\ w_{0,x} + \varphi_x \end{Bmatrix}; \boldsymbol{\gamma}_1 = -\frac{5}{h^2}\begin{Bmatrix} w_{0,y} + \varphi_y \\ w_{0,x} + \varphi_x \end{Bmatrix}. \quad (6)$$

The stress resultants are defined by

$$\begin{bmatrix} \mathbf{N} & \mathbf{M} & \mathbf{P} \end{bmatrix}^T = \mathbf{D}_m \begin{bmatrix} \boldsymbol{\varepsilon}_m & \kappa_1 & \kappa_2 \end{bmatrix}^T; \begin{bmatrix} \mathbf{Q} & \mathbf{R} \end{bmatrix}^T = \mathbf{D}_s \begin{bmatrix} \boldsymbol{\gamma}_0 & \boldsymbol{\gamma}_1 \end{bmatrix}^T \quad (7)$$

where

$$\mathbf{D}_m = \begin{bmatrix} \mathbf{A} & \mathbf{B} & \mathbf{B}^b \\ \mathbf{B} & \mathbf{F} & \mathbf{F}^b \\ \mathbf{B}^b & \mathbf{F}^b & \mathbf{H} \end{bmatrix}; \mathbf{D}_s = \begin{bmatrix} \mathbf{A}^s & \mathbf{B}^s \\ \mathbf{B}^s & \mathbf{F}^s \end{bmatrix} \quad (8)$$

with

$$\left(\mathbf{A}, \mathbf{B}, \mathbf{B}^b, \mathbf{F}, \mathbf{F}^b, \mathbf{H}\right) = \int_{-h/2}^{h/2} \frac{E(z)}{1-\nu(z)^2} \begin{bmatrix} 1 & \nu(z) & 0 \\ \nu(z) & 1 & 0 \\ 0 & 0 & \dfrac{1}{2(1-\nu(z))} \end{bmatrix} (1, z^1, z^3, z^4, z^6) dz;$$
$$\left(\mathbf{A}^s, \mathbf{B}^s, \mathbf{F}^s\right) = \int_{-h/2}^{h/2} \frac{E(z)}{2(1+\nu(z))} \begin{bmatrix} 1 & 0 \\ 0 & 1 \end{bmatrix} (1, z^2, z^4) dz \quad (9)$$

2.3. Finite element procedure

Using the Q4 element with seven DOFs for each node, the nodal displacement vector is determined by [9]:

$$\mathbf{q}_e = \begin{bmatrix} \mathbf{q}_1^T & \mathbf{q}_2^T & \mathbf{q}_3^T & \mathbf{q}_3^T \end{bmatrix}^T \quad (10)$$

with $\mathbf{q}_i \left(i = 1 \div 4\right)$ is the node displacements expressed by

$$\mathbf{q}_i = \begin{Bmatrix} u_{0i} & v_{0i} & w_i & \varphi_{xi} & \varphi_{yi} & \theta_{xi} = \varphi_{xi} + w_{i,x} & \theta_{yi} = \varphi_{yi} + w_{i,y} \end{Bmatrix} \quad (11)$$

Following Hamilton's principle, the motion equation of the sandwich plate element is defined by [25]:

$$\mathbf{M}_e \ddot{\mathbf{q}}_e + \mathbf{K}_e \mathbf{q}_e = \mathbf{F}_e \quad (12)$$

where the element stiffness matrix $\mathbf{K}_e$ is:

$$\mathbf{K}_e = \int_S \left(\begin{Bmatrix} \mathbf{B}_1 \\ \mathbf{B}_2 \\ \mathbf{B}_3 \\ \mathbf{B}_4 \\ \mathbf{B}_5 \end{Bmatrix}^T \begin{bmatrix} \mathbf{A} & \mathbf{B} & \mathbf{B}^b & \mathbf{0} \\ \mathbf{B} & \mathbf{F} & \mathbf{F}^b & \mathbf{0} \\ \mathbf{B}^b & \mathbf{F}^b & \mathbf{H} & \mathbf{0} \\ \mathbf{0} & \mathbf{0} & \mathbf{A}^s & \mathbf{B}^s \\ \mathbf{0} & \mathbf{0} & \mathbf{B}^s & \mathbf{F}^s \end{bmatrix} \begin{Bmatrix} \mathbf{B}_1 \\ \mathbf{B}_2 \\ \mathbf{B}_3 \\ \mathbf{B}_4 \\ \mathbf{B}_5 \end{Bmatrix} \right) dS \tag{13}$$

The element mass matrix $\mathbf{M}_e$ is:

$$\mathbf{M}_e = \int_S \mathbf{N}^T \mathrm{M} \mathbf{N} dS \tag{14}$$

The element load vector $\mathbf{F}_e$ is:

$$\mathbf{F}_e = \int_S \mathbf{N}^T \mathbf{p} dS \tag{15}$$

where $\mathbf{p} = \{0\ 0\ p(t)\ 0\ 0\ 0\ 0\}^T$. The matrices $\mathbf{B}_1, \mathbf{B}_2, \mathbf{B}_3, \mathbf{B}_4, \mathbf{B}_5, \mathrm{M}$, and $\mathbf{N}$ can be found in [26].

The types of boundary conditions (BCs) are defined by:

- Clamped (C): $u_0 = v_0 = w_0 = \varphi_x = \varphi_y = \theta_x = \theta_y = 0$ for all edges;

- Simply supported (S):

$u_0 = w = \varphi_x = \theta_x = 0$ at $y = 0$, $y = b$;

$v_0 = w = \varphi_y = \theta_y = 0$ at $x = 0$, $x = a$.

- Free (F): All DOFs is different from zero.

Now, the motion equation of the h-FGS plate is:

$$\mathbf{M}\ddot{\mathbf{q}} + \mathbf{K}\mathbf{q} = \mathbf{F} \tag{16}$$

where $\mathbf{K} = \sum_{nel} \mathbf{K}_e; \mathbf{M} = \sum_{nel} \mathbf{M}_e; \mathbf{F} = \sum_{nel} \mathbf{F}_e$ is the global stiffness matrix, the global mass matrix, and the global load vector of the h-FGS plate, respectively and symbol "*nel*" represents the number of discretized elements of the sandwich plate. To solve Eq. (16), the Newmark direct integral is used [27].

3. Numerical results and discussions

The main purposes of this section as: (1) Verify the reliability of the proposed method; (2) Present new results in dynamic response of h-FGS plates.

3.1. Verification studies

Example 1: An isotropic sandwich plate made of two coating layers and an auxetic honeycomb core is studied. The input data are the following: $h = 0.1\mathrm{m}$; $h_1 = h_3$;

$h_2 = 1.5h_1$; $a = b = 20h$; $E = 69\,\text{GPa}$; $G = 26\,\text{GPa}$; $\nu = 0.33$; $\rho = 2700\,\text{kg/m}^3$; $\lambda_3 = 0.01385$; $\theta = 35°$. It can be seen that the frequencies obtained from the present method converge to a mesh size of 16 × 16 and agrees well with those of Tran et al. [28] used a classical FEM based on the first-order shear deformation theory (FSDT) as shown in Table 3. The resulting frequency is slightly larger than those of Tran et al. [28] due to the use of TSDT. From here, a mesh size of 16 × 16 will be used for the next examples.

Table 3. The first natural frequencies (Hz) of the honeycomb sandwich plate

Method	Meshing	The first natural frequencies (Hz)			
		$\lambda_1 = 0.5$	$\lambda_1 = 1$	$\lambda_1 = 2$	$\lambda_1 = 4$
Present	8 × 8	172.7732	150.0051	151.9516	152.4548
	10 × 10	172.5238	149.7884	151.7321	152.2346
	12 × 12	172.3903	149.6723	151.6145	152.1166
	14 × 14	172.3106	149.6029	151.5443	152.0461
	16 × 16	172.2592	149.5582	151.4989	152.0006
	18 × 18	172.2592	149.5580	151.4988	152.0005
Tran et al. [28]		172.3232	149.7829	151.7055	152.1957

Example 2: Considering the fully simply supported (SSSS) FGM (SUS304/Si_3N_4) square plate under a sudden uniform load with magnitude $q_0(x, y) = 50$ MP. The geometrical dimensions: a = b = 0.2 m, h = 0.025 m, and the time step is taken as $\Delta t = 0.2\,\mu\text{s}$. It can be obseverd that the obtained deflection response agrees well in both shape and value with that of Abuteir et al. [29] using a curved 8-node degenerated shell element as displayed in Fig. 3. From the above examples, it can be concluded that the author's formula and program are accurate and reliable.

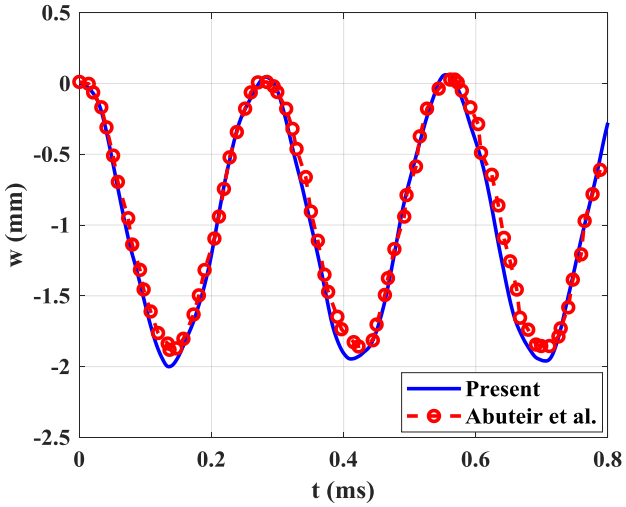

Fig. 3. The deflection response of SSSS FGM square plate centre.

3.2. Free vibration problem

Firstly, Fig. 4 displays the first six mode shapes of the SSSS square h-FGS plate (1-2-1) with the parameters: $a = b = 1$ m, $h = a/25, \lambda_1 = 1, \lambda_3 = 0.1, \theta = 15°, n = 1$.

Secondly, Table 4 shows the first frequency of square h-FGS plates (1-4-1) with parameters such as $h = a/50, \lambda_3 = 0.2, n = 2$ via different values of θ and λ_1. Observing that an increase of θ causes a decrease in the frequency, whereas an increase of λ_1 increases the frequency of h-FGS plates. Furthermore, the obtained frequency of the fully clamped (CCCC) h-FGS plates is higher than that of SSSS h-FGS plates, as expected. Furthermore, Table 7 lists the first six frequencies of square h-FGS plates (2-1-2) with parameters $h = a/75, \lambda_3 = 3, \lambda_3 = 0.3, n = 0.5$.

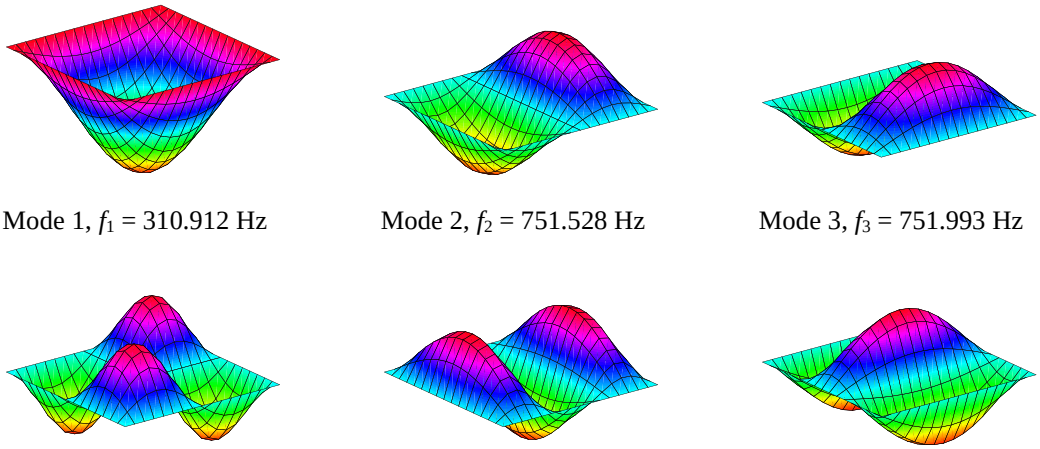

Mode 1, f_1 = 310.912 Hz Mode 2, f_2 = 751.528 Hz Mode 3, f_3 = 751.993 Hz

Mode 4, f_4 = 1168.030 Hz Mode 5, f_5 = 1431.232 Hz Mode 6, f_6 = 1448.400 Hz

Fig. 4. The mode shapes of the SSSS square h-FGS plate.

Table 4. Natural frequencies (Hz) of h-FGS plates via different values of θ and λ_1

θ (Degree)	λ parameter					
	$\lambda_1 = 1$	$\lambda_1 = 1.5$	$\lambda_1 = 2$	$\lambda_1 = 3$	$\lambda_1 = 4$	$\lambda_1 = 4.5$
Boundary condition	SSSS					
15°	151.8017	159.1134	162.584	165.9565	167.62	168.1743
30°	138.4386	152.2291	157.8901	162.9608	165.3243	166.0924
45°	114.449	141.104	150.3276	157.9519	161.3184	162.387
65°	75.9754	123.4605	137.6497	148.9006	153.7502	155.2746
75°	29.9339	94.7971	113.3741	128.9739	136.0166	138.2753
Boundary condition	CCCC					
15°	273.7862	285.9896	291.6882	297.1463	299.807	300.6895
30°	250.7758	274.2403	283.7258	292.1273	296.0105	297.2682
45°	208.3799	254.7816	270.5566	283.4794	289.1576	290.9574
65°	138.9768	223.3751	248.1516	267.6855	276.0969	278.7427
75°	55.0146	171.6975	204.8319	232.684	245.2997	249.3551

Table 5. The first six natural frequencies of h-FGS plates (Hz)

θ (Degree)	*The natural frequency* (Hz)					
	f_1	f_2	f_3	f_4	f_5	f_6
Boundary condition	SSSS					
15°	93.7852	234.8057	234.8127	374.754	471.5708	471.6071
30°	93.3009	233.5727	233.6352	372.8289	469.086	469.2843
45°	92.4357	231.3818	231.5067	369.3886	464.6697	465.0654
65°	90.7209	227.0601	227.27	362.5699	455.9729	456.6555
75°	86.0946	215.4244	215.8258	344.1662	432.5899	433.9133
Boundary condition	CCCC					
15°	171.6825	351.5559	351.5821	517.5133	634.9717	637.8941
30°	170.8046	349.7194	349.8417	514.8877	631.7566	634.6825
45°	169.2291	346.447	346.6909	510.1835	625.9615	628.9229
65°	166.108	339.994	340.4195	500.8623	614.4523	617.542
75°	493.204	689.673	699.729	867.979	963.220	995.379

3.3. Dynamic response analysis

Firstly, the effect of the thickness ratio ($h_1 - h_2 - h_3$) on the dynamic response of SSSS square h-FGS plates subjected to consecutive blast loading is displayed in Fig. 5. Observing that an increase in a core thickness layer h_2 leads to the deflection response of the h-FGS plate centre increase. Besides, the thicker FGM skin layers contribute to an augmented stiffness of h-FGS plates, and protect the inner honeycomb core.

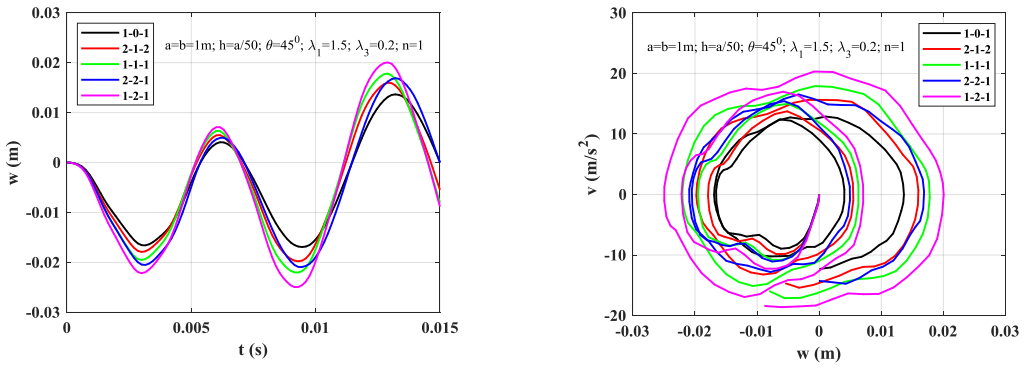

a) The central deflection history *b) The phase orbit*

Fig. 5. The dynamic response of SSSS h-FGS plates as function of thickness ratio layers.

Next, Fig. 6 shows the influence of λ_1 on the dynamic response of SSSS square h-FGS plates (1-1-1). Observing that an increase in λ_1 results in an increase in the deflection response of the h-FGS plate during the first wave. In the next stage, the opposite is true when the second wave begins to act on the plate. This may be due to the self-oscillation of the structure at the time the second wave layer starts to act. The phase diagrams are very tangled lines due to the impact of the blast wave and the honeycomb core.

Finally, Fig. 7 shows the impact of θ on the dynamic response of CCCC square h-FGS plates (2-1-2). Observing that there is no general rule to describe the influence of θ on the dynamic response of h-FGS plates. In general, the parameters of the auxetic unit cell have a mutual influence on the stiffness of sandwich plates. Moreover, from the phase trajectory graph, it can be seen that the vibration properties of the plate are complex, the curves are not smooth and not closed. Besides, the Firstly, the effect of the thickness ratio ($h_1 - h_2 - h_3$) on the dynamic response of SSSS square h-FGS plates subjected to the consecutive blast loading is displayed in Fig. 5 also makes the vibrations of sandwich plates more complex and unpredictable.

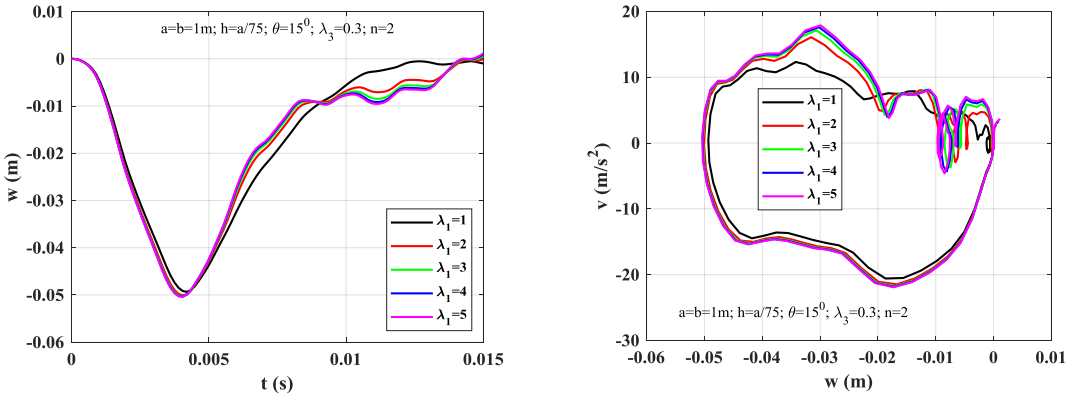

a) The central deflection history *b) The phase orbit*

Fig. 6. The dynamic response of SSSS h-FGS plates as function of λ_1.

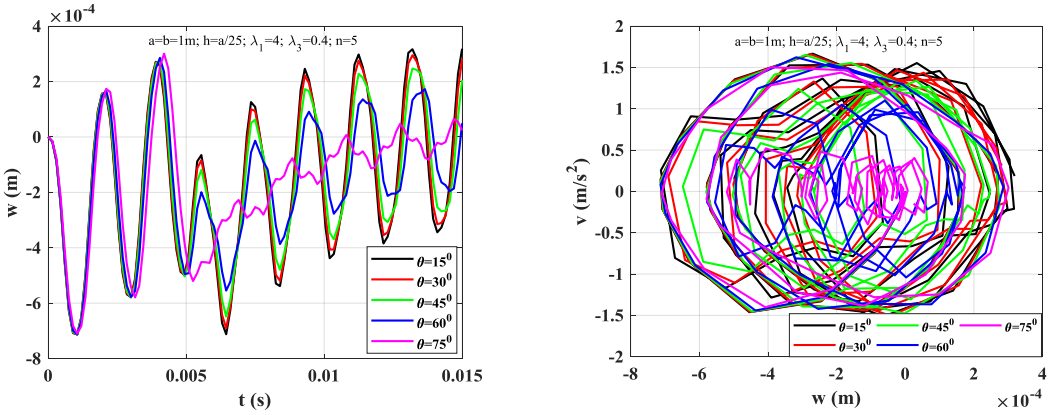

a) The central deflection history *b) The phase orbit*

Fig. 7. The dynamic response of CCCC h-FGS plates as function of θ.

4. Conclusions

The main goal of this article is to study the dynamic response of h-FGS plates by the Q4 element with seven DOFs per node within the framework of Hamilton's principle. The accuracy and reliability of the proposed method are verified through comparative

examples. Besides, the article also examines the effect of material properties and geometric parameters on the dynamic response of h-FGS plates. From here, the key findings from this research can be summarized as follows:

- Using the Q4 element combined with Shi's TSDT simplifies the discretization of the problem domain, even for complex geometric shapes.

- The obtained results reveal the intricate influence of the auxetic unit cell of the honeycomb core on the dynamic response of h-FGS plates. Additionally, employing FGM skin layers enhances the stiffness of the h-FGS plates and protects the honeycomb core against blast loading.

- The consecutive blast loading has a complex effect on the dynamic response of the h-FGS plate.

- The obtained findings in this study have significant potential to assist in the design of practical h-FGS plates.

- Optimizing the shape and size of the honeycomb core opens up a potential direction for future research.

References

[1] K. Ha, "Finite element analysis of sandwich plates: An overview", *Computers & Structures*, Vol. 37, No. 4, pp. 397-403, 1990. DOI: 10.1016/0045-7949(90)90028-Z

[2] H. Wan, H. Ohtaki, S. Kotosaka, and G. Hu, "A study of negative Poisson's ratios in auxetic honeycombs based on a large deflection model", *European Journal of Mechanics-A/Solids*, Vol. 23, No. 1, pp. 95-106, 2004. DOI: 10.1016/j.euromechsol.2003.10.006

[3] X. C. Zhang, L. Q. An, H. M. Ding, X. Y. Zhu, and M. El-Rich, "The influence of cell micro-structure on the in-plane dynamic crushing of honeycombs with negative Poisson's ratio", *Journal of Sandwich Structures & Materials*, Vol. 17, No. 1, pp. 26-55, 2015. DOI: 10.1177/1099636214554180

[4] X. Zhu, J. Zhang, W. Zhang, and J. Chen, "Vibration frequencies and energies of an auxetic honeycomb sandwich plate", *Mechanics of Advanced Materials and Structures*, Vol. 26, No. 23, pp. 1951-1957, 2019. DOI: 10.1080/15376494.2018.1455933

[5] D. D. Nguyen and C. H. Pham, "Nonlinear dynamic response and vibration of sandwich composite plates with negative Poisson's ratio in auxetic honeycombs", *Journal of Sandwich Structures & Materials*, Vol. 20, No. 6, pp. 692-717, 2018. DOI: 10.1177/1099636216674729

[6] N. D. Duc, K. Seung-Eock, P. H. Cong, N. T. Anh, and N. D. Khoa, "Dynamic response and vibration of composite double curved shallow shells with negative Poisson's ratio in auxetic honeycombs core layer on elastic foundations subjected to blast and damping loads", *International Journal of Mechanical Sciences*, Vol. 133, pp. 504-512, 2017. DOI: 10.1016/j.ijmecsci.2017.09.009

[7] P. H. Cong, N. D. Khanh, N. D. Khoa, and N. D. Duc, "New approach to investigate nonlinear dynamic response of sandwich auxetic double curves shallow shells using TSDT", *Composite Structures*, Vol. 185, pp. 455-465, 2018. DOI: 10.1016/j.compstruct.2017.11.047

[8] T. T. Tran, Q. H. Pham, T. T. Nguyen, and T. V. Tran, "Dynamic analysis of sandwich auxetic honeycomb plates subjected to moving oscillator load on elastic foundation", *Advances in Materials Science and Engineering*, Vol. 2020, pp. 1-16, 2020. DOI: 10.1155/2020/6309130

[9] Q. H. Pham, P. C. Nguyen, T. T. Tran, and T. Nguyen-Thoi, "Free vibration analysis of nanoplates with auxetic honeycomb core using a new third-order finite element method and nonlocal elasticity theory", *Engineering with Computers*, 2021, pp. 1-19. DOI: 10.1007/s00366-021-01531-3

[10] N. V. Nguyen, H. Nguyen-Xuan, T. N. Nguyen, J. Kang, and J. Lee, "A comprehensive analysis of auxetic honeycomb sandwich plates with graphene nanoplatelets reinforcement", *Composite Structures*, Vol. 259, 2021, 113213. DOI: 10.1016/j.compstruct.2020.113213

[11] Q. H. Pham, P. C. Nguyen, and T. T. Tran, "Free vibration response of auxetic honeycomb sandwich plates using an improved higher-order ES-MITC3 element and artificial neural network", *Thin-Walled Structures*, Vol. 175, 2022, 109203. DOI: 10.1016/j.tws.2022.109203

[12] N. T. Thang, N. V. Long, T. M. Tu, N. H. Nam, and M. C. Anh, "Navier solution for static and free vibration analysis of sandwich plate with auxetic honeycomb core resting on pasternak elastic foundation", *Journal of Science and Technology in Civil Engineering (STCE)-HUCE*, Vol. 16, No. 3, pp. 18-28, 2022. DOI: 10.31814/stce.huce(nuce)2022-16(3)-02

[13] F. Y. Addou, F. Bourada, M. Meradjah, …, A. Alnujaie, "Impact of porosity distribution on static behavior of functionally graded plates using a simple quasi-3D HSDT", *Computers and Concrete*, Vol. 32, No. 1, pp. 87-97, 2023. DOI: 10.12989/cac.2023.32.1.087

[14] V. L. Nguyen, M. T. Tran, S. Limkatanyu, and J. Rungamornrat, "Free vibration analysis of rotating FGP sandwich cylindrical shells with metal-foam core layer", *Mechanics of Advanced Materials and Structures*, 2022, pp. 1-14. DOI: 10.1080/15376494.2022.2073410

[15] N. Lam, P. Mendis, and T. Ngo, "Response spectrum solutions for blast loading", *Electronic Journal of Structural Engineering*, Vol. 4, pp. 28-44, 2004. DOI: 10.56748/ejse.439

[16] G. Imbalzano, P. Tran, T. D. Ngo, and P. V. Lee, "A numerical study of auxetic composite panels under blast loadings", *Composite Structures*, Vol. 135, pp. 339-352, 2016. DOI: 10.1016/j.compstruct.2015.09.038

[17] G. Imbalzano, S. Linforth, T. D. Ngo, P. V. S. Lee, and P. Tran, "Blast resistance of auxetic and honeycomb sandwich panels: Comparisons and parametric designs", *Composite Structures*, Vol. 83, pp. 242-261, 2018. DOI: 10.1016/j.compstruct.2017.03.018

[18] S. Li, X. Li, Z. Wang, …, L. Zhao, "Finite element analysis of sandwich panels with stepwise graded aluminum honeycomb cores under blast loading", *Composites Part A: Applied Science and Manufacturing*, Vol. 80, pp. 1-12, 2016. DOI: 10.1016/j.compositesa.2015.09.025

[19] D. D. Nguyen and C. H. Pham, "Nonlinear dynamic response and vibration of sandwich composite plates with negative Poisson's ratio in auxetic honeycombs", *Journal of Sandwich Structures & Materials*, Vol. 20, No. 6, pp. 692-717, 2018. DOI: 10.1177/1099636216674729

[20] N. D. Duc, N. D. Tuan, P. Tran, and T. Q. Quan, "Nonlinear dynamic response and vibration of imperfect shear deformable functionally graded plates subjected to blast and thermal loads", *Mechanics of Advanced Materials and Structures*, Vol. 24, No. 4, pp. 318-329, 2017. DOI: 10.1080/15376494.2016.1142024

[21] C. Qi, S. Yang, L. J. Yang, S. H. Han, and Z. H. Lu, "Dynamic response and optimal design of curved metallic sandwich panels under blast loading", *The Scientific World Journal 2014*, 2014. DOI: 10.1155/2014/853681

[22] F. Bounouara, M. Sadoun, M. M. S. Saleh, ..., A. Tounsi, "Effect of visco-Pasternak foundation on thermo-mechanical bending response of anisotropic thick laminated composite plates", *Steel and Composite Structures*, Vol. 47, pp. 693-707, 2023. DOI: 10.12989/scs.2023.47.6.693

[23] N. T. Do, P. B. Le, T. S. Le, T. T. Tran, and Q. H. Pham, "Vibration characteristics of h-FGS plates resting on an elastic foundation under double blast loading", *Alexandria Engineering Journal*, Vol. 86, pp. 131-43, 2024. DOI: 10.1016/j.aej.2023.11.050

[24] G. Shi, "A new simple third-order shear deformation theory of plates", *International Journal of Solids and Structures*, Vol. 44, pp. 4399-4417, 2007. DOI: 10.1016/j.ijsolstr.2006.11.031

[25] J. N. Reddy, *Mechanics of laminated composite plates and shells: Theory and analysis*, CRC Press, 2003. DOI: 10.1201/b12409

[26] J. Wolf, *Dynamic SoilStructure Interaction*, PrenticeHall. Inc., Englewood Cliffs, New Jersey, 1985.

[27] T. H. Nguyen, T. T. Nguyen, T. T. Tran, and Q. H. Pham, "Research on the mechanical behaviour of functionally graded porous sandwich plates using a new C1 finite element procedure", *Results in Engineering*, Vol. 17, 2023, 100817. DOI: 10.1016/j.rineng.2022.100817

[28] T. T. Tran, Q. H. Pham, T. T. Nguyen, and T. V. Tran, "Dynamic analysis of sandwich auxetic honeycomb plates subjected to moving oscillator load on elastic foundation", *Advances in Materials Science and Engineering*, 2020, pp. 1-16. DOI: 10.1155/2020/6309130

[29] B. Abuteir, E. Harkati, D. Boutagouga, S. Mamouri, and K. Djeghaba, "Thermo-mechanical nonlinear transient dynamic and Dynamic-Buckling analysis of functionally graded material shell structures using an implicit conservative/decaying time integration scheme", *Mechanics of Advanced Materials and Structures*, 2021, pp. 1-20. DOI: 10.1080/15376494.2021.1964115

PHÂN TÍCH ĐÁP ỨNG ĐỘNG CỦA TẤM h-FGS CHỊU TẢI TRỌNG HAI SÓNG NỔ LIÊN TIẾP

Dương Mạnh Tuấn[1]

[1]*Viện Kỹ thuật Công binh, Sa Đôi, Hà Nội, Việt Nam*

Tóm tắt: Mục đích chính của bài báo này là sử dụng phương pháp phần tử hữu hạn (PTHH) dựa trên lý thuyết biến dạng cắt bậc ba (TSDT) của Shi để phân tích đáp ứng động của tấm sandwich với lõi tổ ong auxetic và hai lớp da làm bằng vật liệu phân lớp chức năng (FGM) (gọi là tấm h-FGS) chịu tải trọng hai sóng nổ liên tiếp. Phương trình chuyển động của tấm được rút ra từ nguyên lý Hamilton. Sau khi xác minh độ tin cậy của phương pháp đề xuất, ảnh hưởng của các thông số hình học và tính chất vật liệu đến đáp ứng động của tấm h-FGS được tiến hành một cách chi tiết. Kết quả thu được hy vọng sẽ hữu ích cho việc tính toán và thiết kế tấm h-FGS trong thực tế kỹ thuật.

Từ khóa: *Đáp ứng động; FGM; lõi tổ ong; PTHH.*

Received: 21/02/2024; Revised: 12/06/2024; Accepted for publication: 28/06/2024

❑